

Electronic Supplementary Information (ESI)

High-Efficiency Zirconium-Based Single-Atom Catalyst for the Transformation of Biomass-Derived 5-Hydroxymethylfurfural to 2,5-Bis(hydroxymethyl)furan with Nearly 100% Selectivity

Lei Hu,^{*a,‡} Aiyong He,^{a,‡} Xinming Shen,^a Qinyin Gu,^a Jingyi Zheng,^a Zhen Wu,^a Yetao

Jiang,^a Xiaoyu Wang,^a Jiaying Xu,^a Yuhe Kan^{*b} and Feng Xu^{*c}

^a Jiangsu Key Laboratory for Biomass-Based Energy and Enzyme Technology, School of Chemistry and Chemical Engineering, Huaiyin Normal University, Huaian 223300, China

^b Jiangsu Key Laboratory for Chemistry of Low-Dimensional Materials, School of Chemistry and Chemical Engineering, Huaiyin Normal University, Huaian 223300, China

^c Beijing Key Laboratory of Lignocellulosic Chemistry, College of Materials Science and Technology, Beijing Forestry University, Beijing 100083, China

* Corresponding Author: hulei@hytc.edu.cn; kyh@hytc.edu.cn; xfx315@bjfu.edu.cn

‡ These authors contributed equally to this work.

Experimental materials

5-Hydroxymethylfurfural (HMF, 98%) and 2,5-bis(hydroxymethyl)furan (BHMF, 98%) were supplied by Saen Chemical Technology Co., Ltd. (Shanghai, China). Zirconium oxide (ZrO_2 , 99%), zirconium nitrate pentahydrate ($Zr(NO_3)_4 \cdot 5H_2O$, 99%), zinc nitrate hexahydrate ($Zn(NO_3)_2 \cdot 6H_2O$, 99%), copper nitrate hexahydrate ($Cu(NO_3)_2 \cdot 6H_2O$, 99%), cobalt nitrate hexahydrate ($Co(NO_3)_2 \cdot 6H_2O$, 99%) and 2-methylimidazole (MIM, 99%) were purchased from Shanghai Aladdin Reagent Co., Ltd. (Shanghai, China). The deuterated isopropanol-OD (*i*PrOH-OD, 98% D) and isopropanol-D₈ (*i*PrOH-D₈, 99% D) were supplied by J&K Scientific Co., Ltd. (Shanghai, China). Methanol (MeOH), ethanol (EtOH), isopropanol (*i*PrOH), *n*-butanol (*n*BuOH), *sec*-butanol (*s*BuOH), formic acid (HCOOH), potassium thiocyanate (KSCN) and other chemicals were purchased from Sinopharm Chemical Reagent Co., Ltd. (Shanghai, China) and used without any purification.

Catalyst characterization

X-ray diffraction (XRD) patterns were performed on a Bruker D8 Advance diffractometer with a Cu K α radiation source ($\lambda=0.15418$ nm). Fourier transform infrared (FT-IR) spectra were recorded on a Nicolet 380 spectrometer. Nitrogen adsorption-desorption (NAD) isotherms were measured on a Micromeritics ASAP 2020 physisorption analyzer at 77 K. Scanning electron microscopy (SEM), high-resolution transmission electron microscopy (HR-TEM) and high-angle annular dark-field scanning transmission electron microscopy (HAADF-STEM) images were carried out on a Zeiss Supra55 microscope, a JEM-2100f microscope and a FEI Titan Themis

G2 60-300 microscope with a spherical aberration corrector, respectively. Element contents were determined by a VISTA-MPX inductively coupled plasma atomic emission spectrometer (ICP-AES) and a Vario EL III elemental analyzer (EA), respectively. X-ray photoelectron spectroscopy (XPS), ultraviolet photoelectron spectroscopy (UPS) and pyridine-adsorbed FT-IR spectra were collected on an Escalab 250Xi spectrometer with an Al K α excitation source ($h\nu = 1486.6$ eV), a Thermo Nexsa G2 spectrometer with a He excitation source ($\phi = 21.22$ eV) and a Bruker Tensor27 spectrometer in the range of 1300 to 1700 cm^{-1} , respectively. X-ray absorption structure (XAS) spectra were obtained at the 1W1B station in Beijing Synchrotron Radiation Facility (BSRF, China). The electron storage ring was monochromatized by a Si (111) double-crystal monochromator and operated at 3.5 GeV with a maximum current of 250 mA. Zr foil and ZrO₂ were used as the standard reference samples, and data collection was collected in transmission mode. The data of X-ray absorption near-edge structure (XANES) and extended X-ray absorption fine structure (EXAFS) was analyzed by Athena module and Artemis module in Demeter software packages, respectively, and the corresponding technical support was provided by Zhengzhou Mice Technology Co., Ltd. (Zhengzhou, China).

Product analysis

HMF and BHMF were analyzed by gas chromatography (GC, Shimadzu GC-2014) and gas chromatography-mass spectrometer (GC-MS, Shimadzu QP2010). For GC and GC-MS analysis, the injector temperature and detector temperature were set to 300 °C. Meanwhile, the initial column temperature was 40 °C and maintained for 2 min,

and then, the column temperature was elevated to 100 °C with a heating rate of 5 °C/min and maintained for 2 min, after that, the column temperature was further elevated to 250 °C with a heating rate of 10 °C/min and maintained for 1 min. Moreover, HMF conversion, BHMF yield and BHMF selectivity were based on the external standard method and calculated by means of the following equations:

$$\text{HMF conversion (\%)} = \left(1 - \frac{\text{Mole of HMF in products}}{\text{Initial mole of HMF}}\right) \times 100 \quad (1)$$

$$\text{BHMF yield (\%)} = \frac{\text{Mole of BHMF in products}}{\text{Initial mole of HMF}} \times 100 \quad (2)$$

$$\text{BHMF selectivity (\%)} = \frac{\text{BHMF yield}}{\text{HMF conversion}} \times 100 \quad (3)$$

Isotope labelling

To explore the reaction mechanism for the TH of HMF to BHMF over Zr/NC, the isotope labelling study was performed in *i*PrOH-D₈. After different reaction times, the reaction products were qualitatively analyzed by nuclear magnetic resonance spectrometer (NMR, JEOL ECX-500) and gas chromatography mass spectrometer (GC-MS, Agilent 7890B-5977A) equipped with a HP-5MS capillary column (30 m × 0.25 mm × 0.25 μm).

Catalyst recovery

To investigate the recyclability of Zr/NC, when each reaction run was completed, the catalyst was separated by filtration from the reaction mixture, and washed with the deionized water (DW) and EtOH for five times, respectively. After drying in a vacuum oven at 80 °C for 12 h, the recovered catalyst was directly used for the next reaction run under the same reaction conditions.

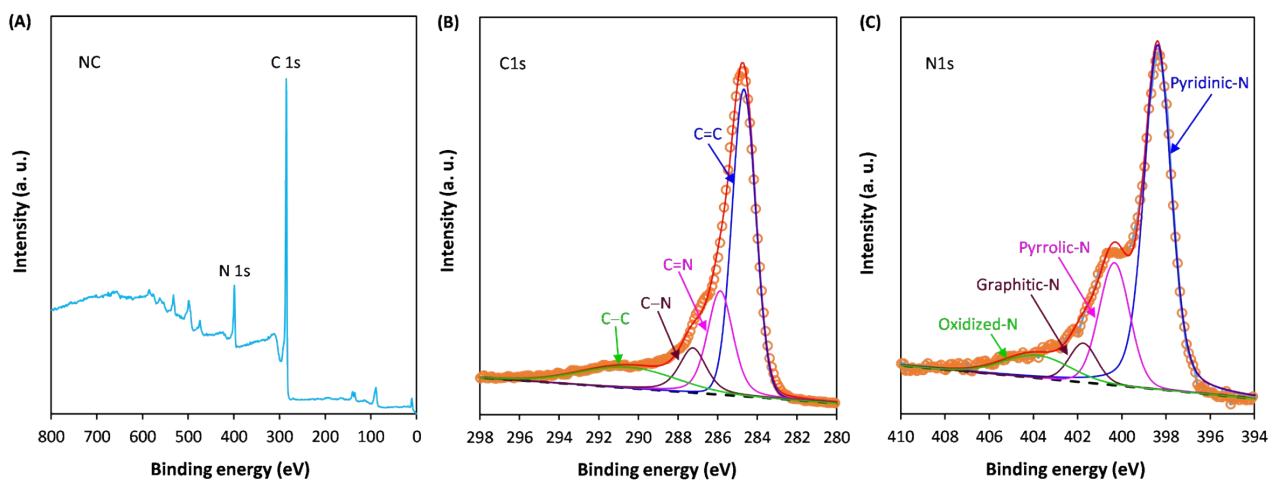


Fig. S1 XPS survey scan spectrum of NC (A) with high-resolution spectra of C 1s (B) and N 1s (C).

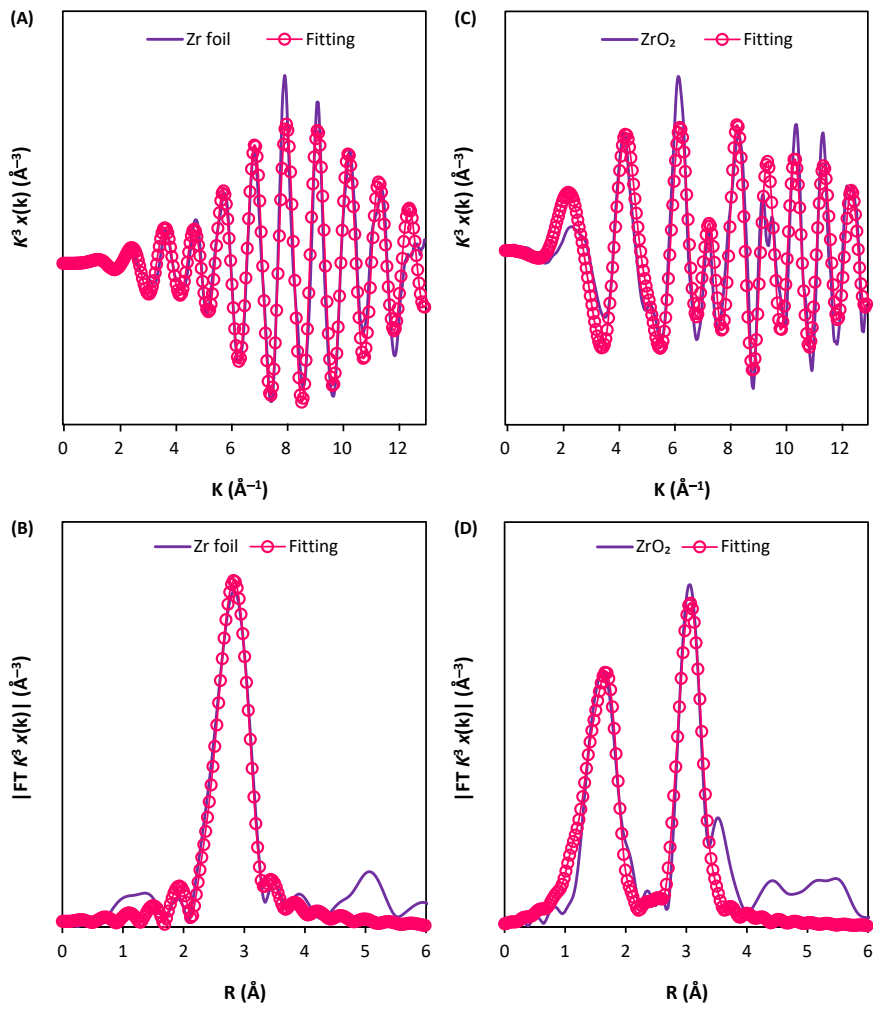


Fig. S2 Zr K-edge EXAFS fitting curves of Zr foil (A~B) and ZrO₂ (C~D).

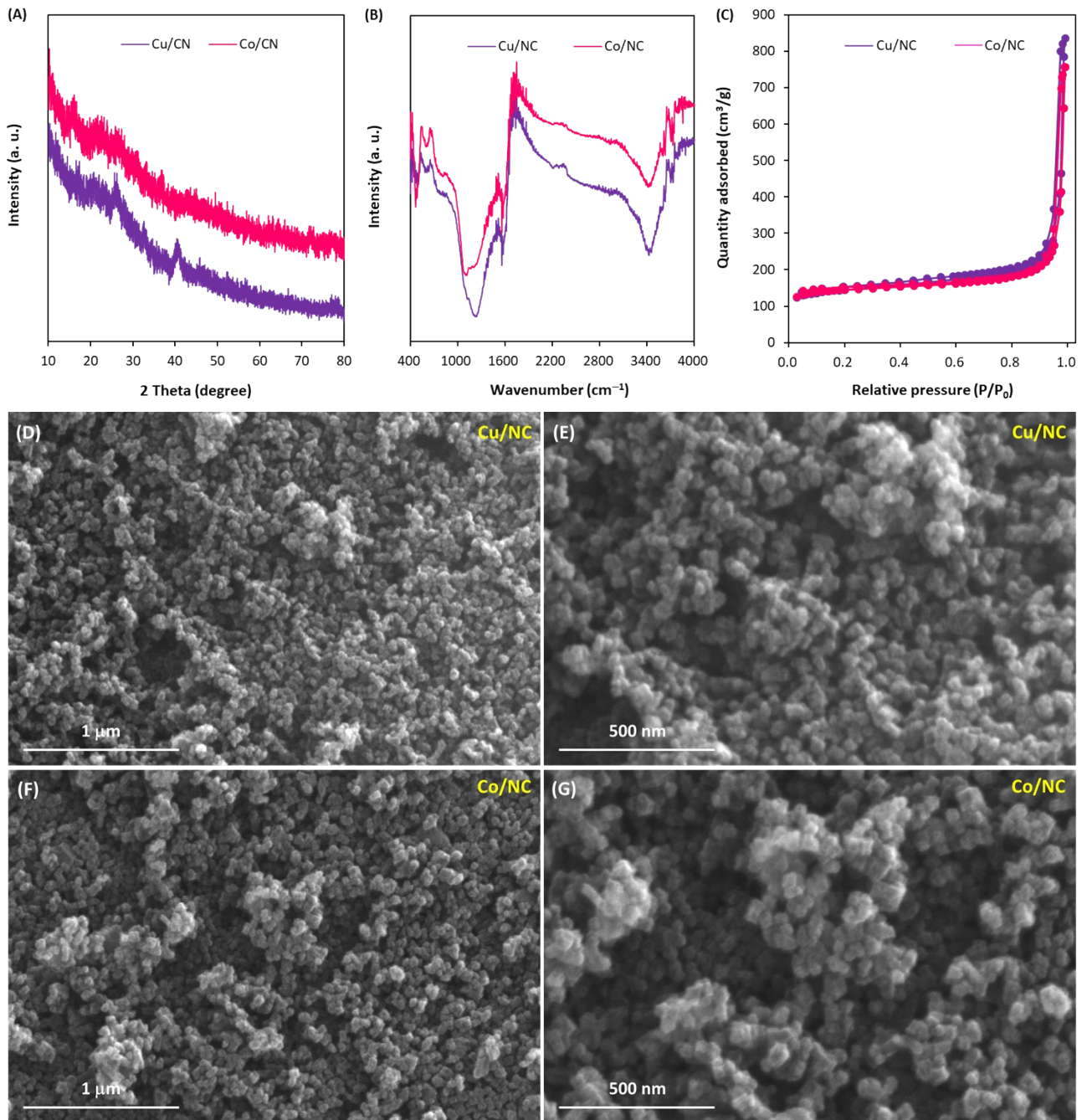


Fig. S3 XRD patterns (A), FT-IR spectra (B), NAD isotherms (C) and SEM images (D~G) of Cu/NC and Co/NC.

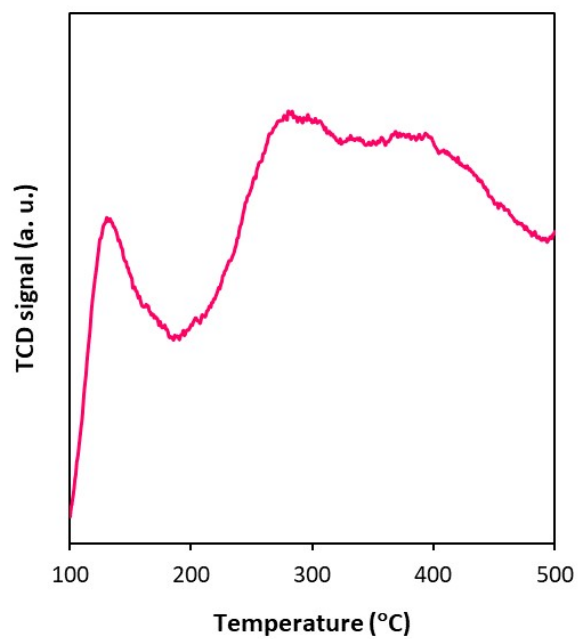


Fig. S4 CO₂-TPD pattern of NC.

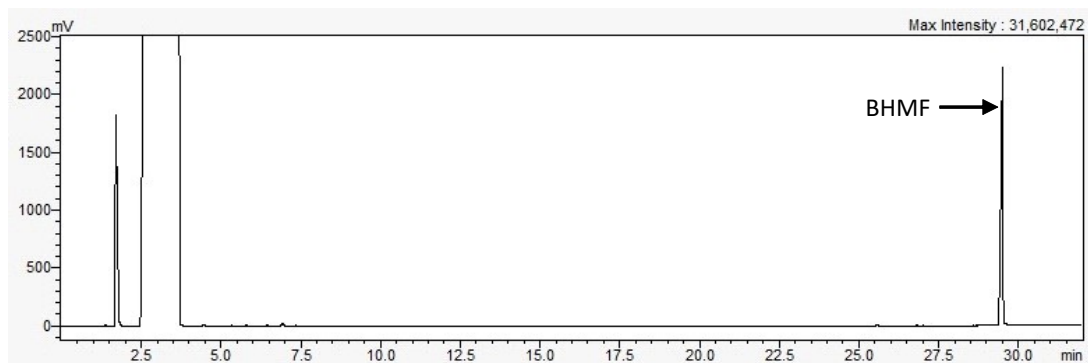


Fig. S5 GC chromatogram for the TH of HMF to BHMF over Zr/NC in *i*PrOH. Reaction conditions: 0.25 g HMF, 19.75 g *i*PrOH, 0.1 g Zr/NC, 130 °C, 150 min.

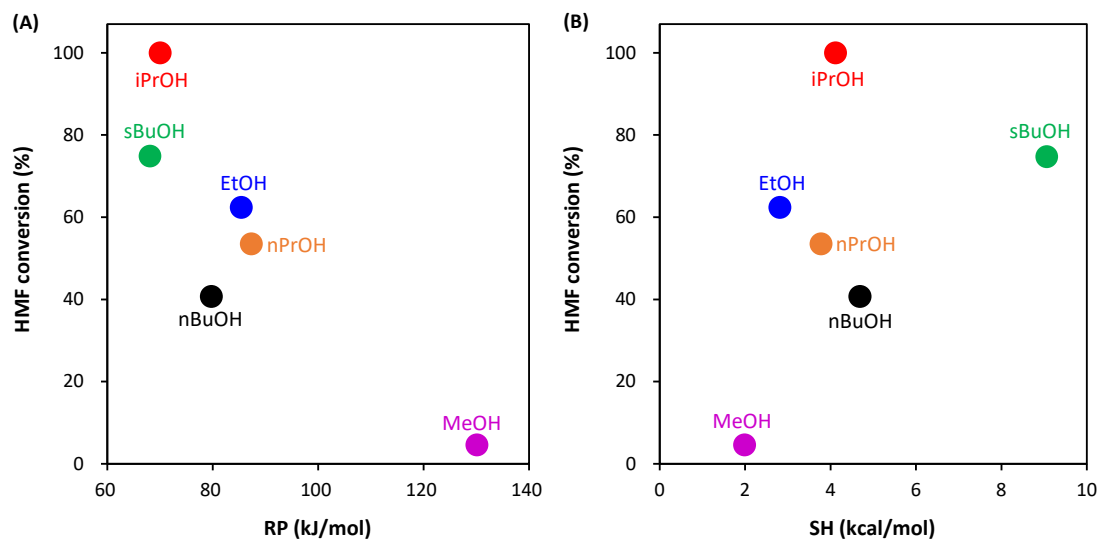


Fig. S6 Correlations of HMF conversion with the RPs (A) and SHs (B) of HDs. Reaction

conditions: 0.25 g HMF, 19.75 g *i*PrOH, 0.1 g Zr/NC, 130 °C, 150 min.

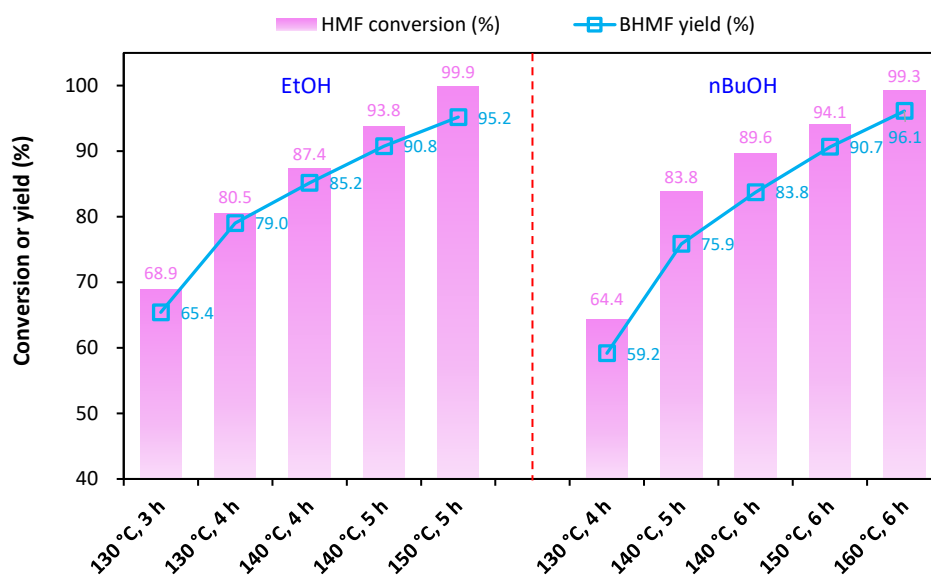


Fig. S7 Optimization of reaction conditions for the TH of HMF to BHMf over Zr/NC in EtOH and *n*BuOH. Reaction conditions: 0.25 g HMF, 19.75 g alcohol, 0.1 g Zr/NC.

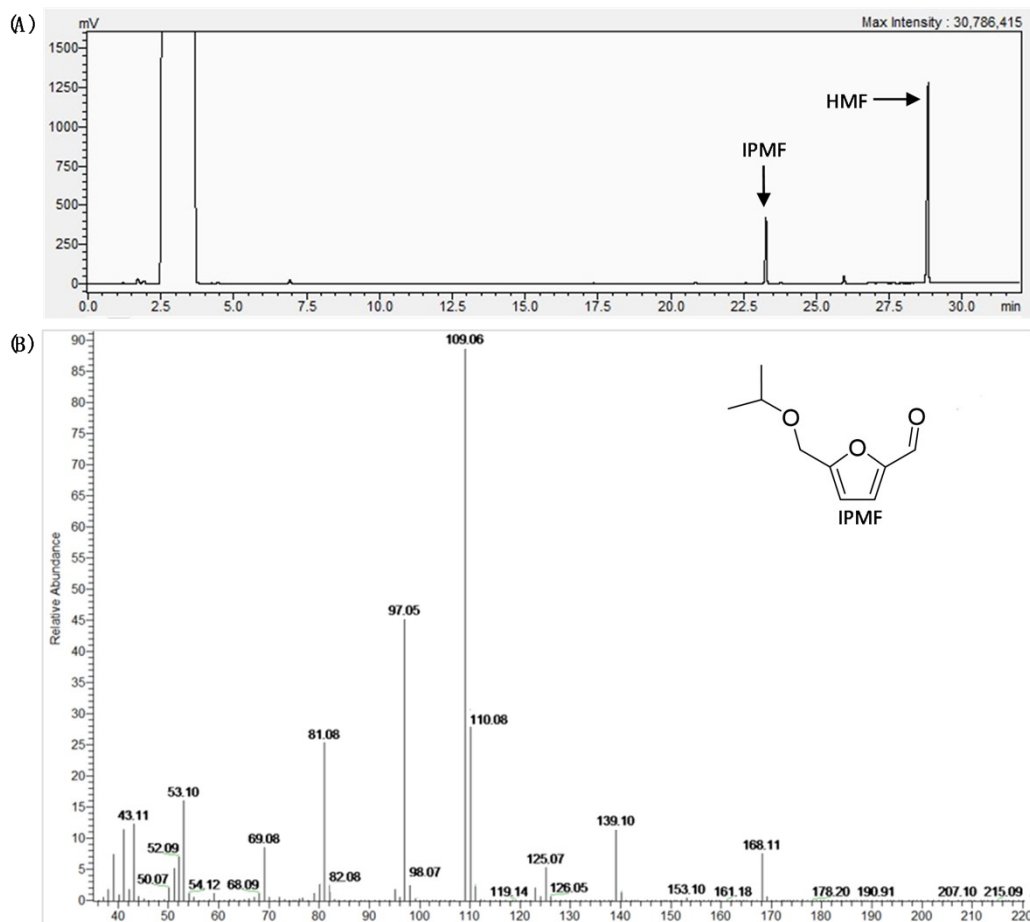


Fig. S8 (A) GC chromatogram for the TH of HMF over 5Zr/NC in *i*PrOH. Reaction conditions: 0.25 g HMF, 19.75 g *i*PrOH, 0.1 g Zr/NC, 130 °C, 150 min. (B) MS spectrum of IPMF.

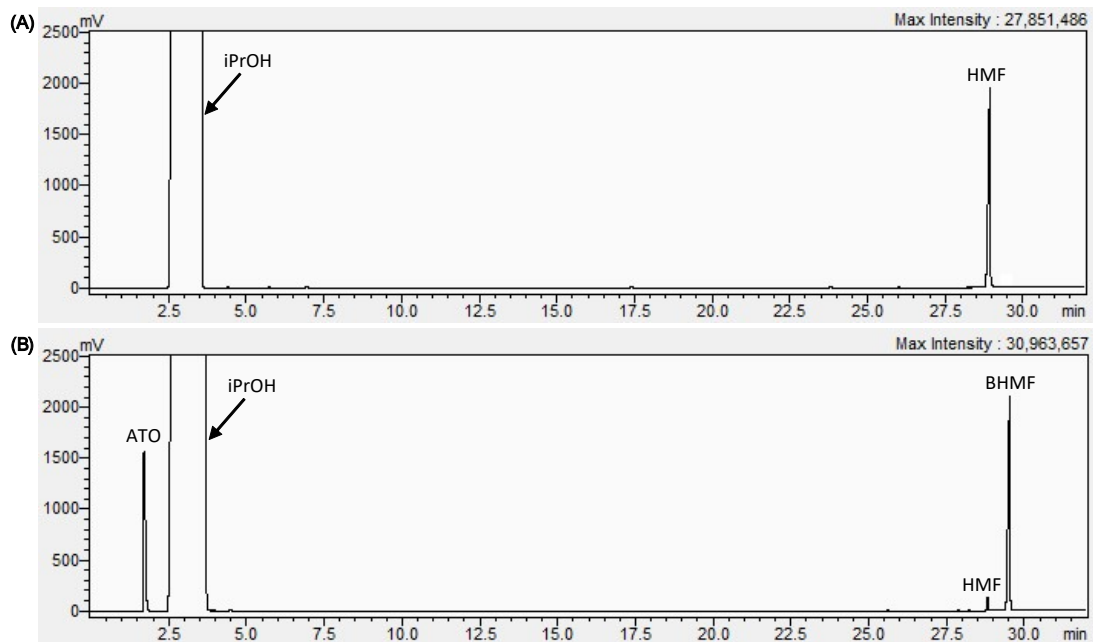


Fig. S9 GC chromatograms for the TH of HMF in *i*PrOH. Reaction conditions: (A) 0.25 g HMF, 19.75 g *i*PrOH, 130 °C, 120 min. (B) 0.25 g HMF, 19.75 g *i*PrOH, 0.1 g Zr/NC, 130 °C, 120 min.

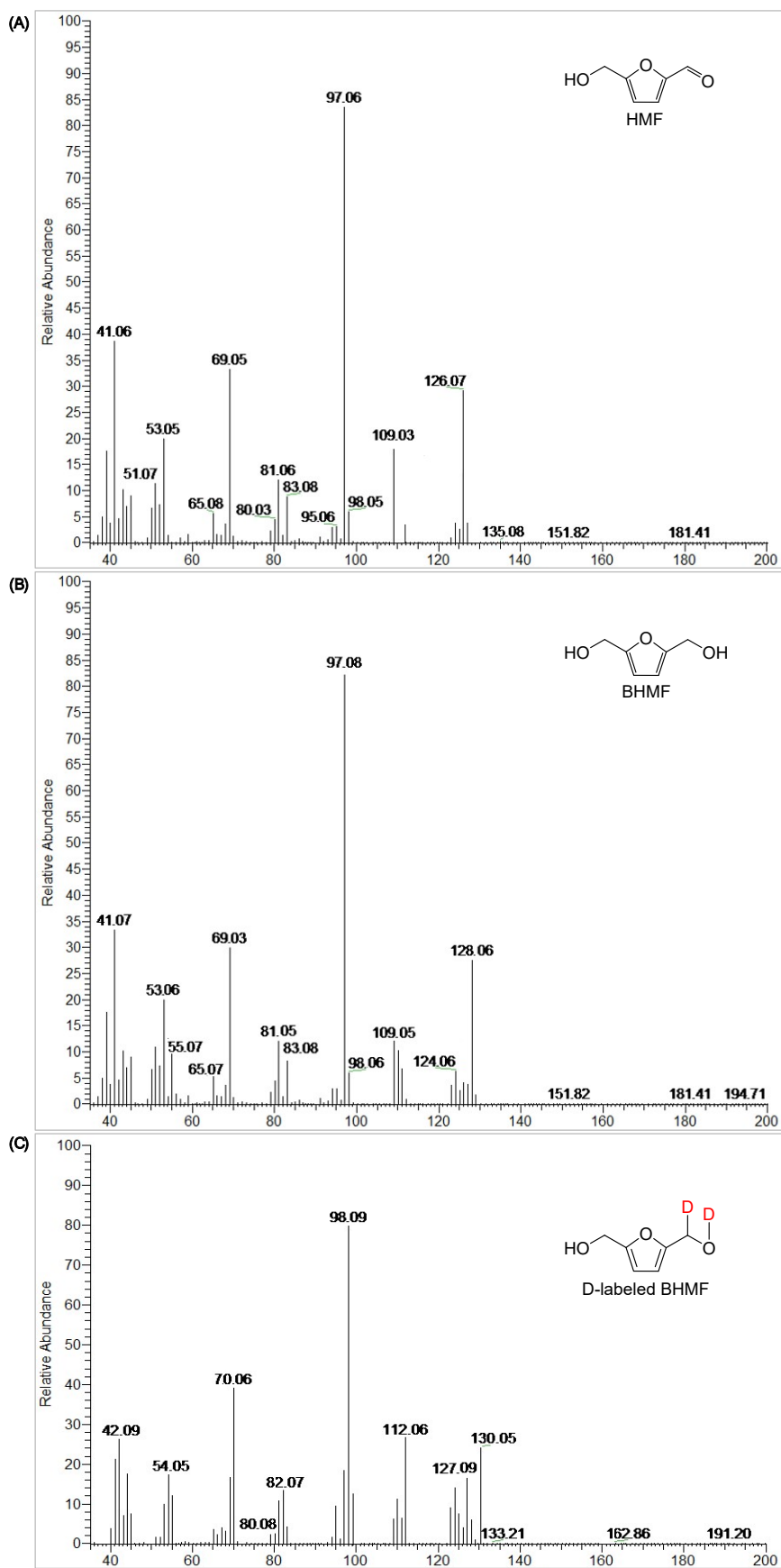


Fig. S10 MS spectra of HMF (A), BHMf (B) and D-labeled BHMf (C).

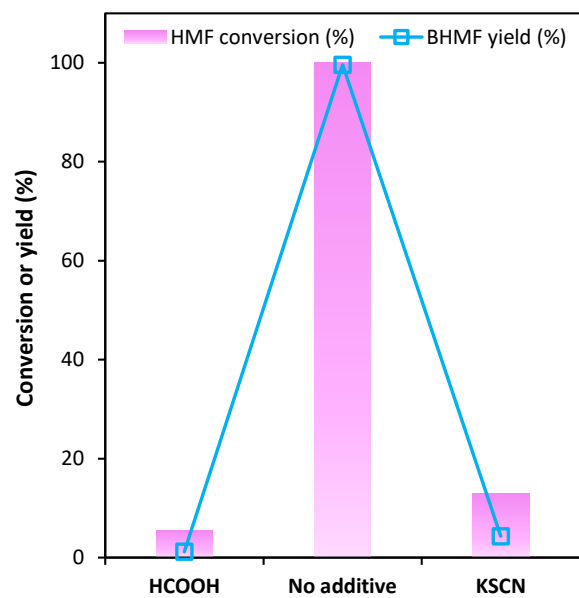


Fig. S11 TH of HMF to BHMf in *i*PrOH over Zr/NC with the addition of various additives. Reaction conditions: 0.25 g HMF, 19.75 g *i*PrOH, 0.1 g Zr/NC, 0.05 g additive, 130 °C, 150 min.

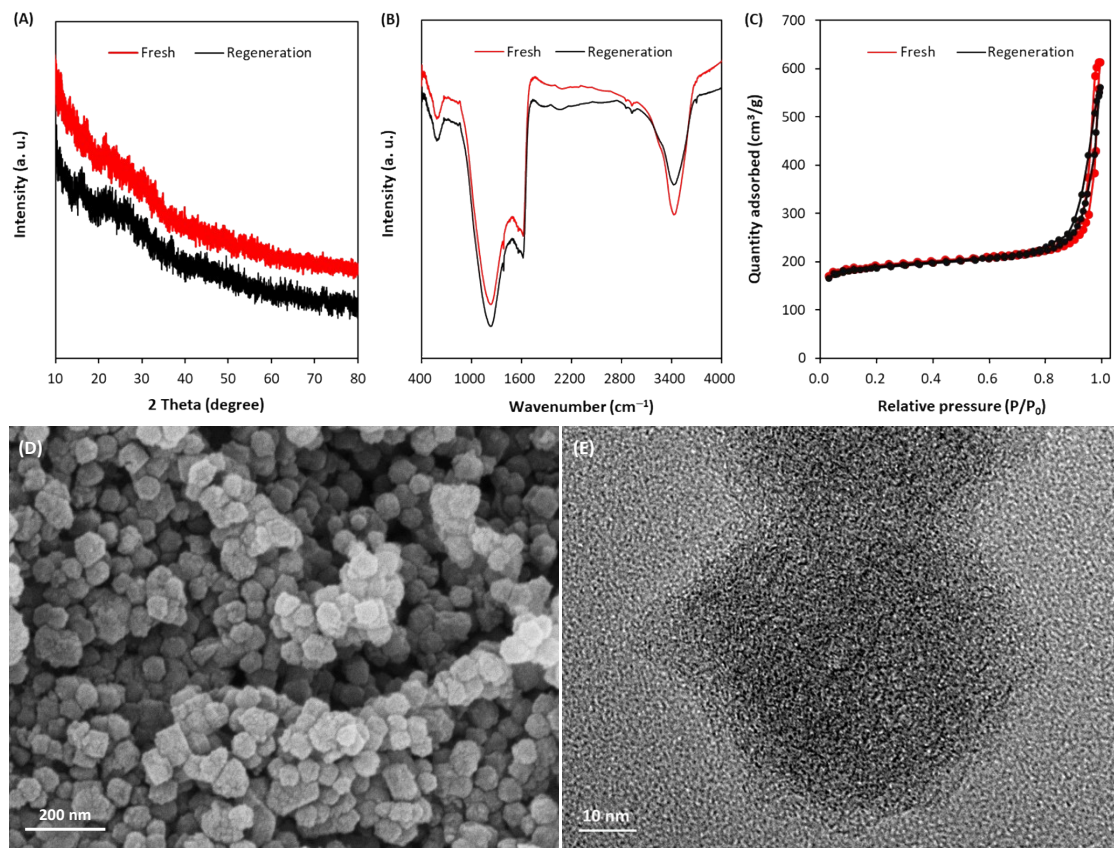


Fig. S12 (A) XRD pattern, (B) FT-IR spectrum, (C) NAD isotherm, (D) SEM image and (E)

TEM image of the regenerated Zr/NC.

Table S1 Characterization results of various catalysts.

Catalyst	Specific surface area (m ² /g)	Pore size (nm)	Pore volume (cm ³ /g)
ZIF-8	1360	3.3	0.628
Zr@ZIF-8	1394	2.4	0.644
NC	576	3.4	0.698
Zr/NC	614	5.8	0.716
Cu/NC	484	10.3	1.146
Co/NC	471	9.1	0.991

Table S2 Zr K-edge EXAFS fitting parameters ($S_0^2=0.95$).

Sample	Path	CN	R (Å)	σ^2 (10^{-3} Å ²)	ΔE (eV)	R factor
Zr foil	Zr–Zr	12	3.21±0.01	9.4±0.7	-7.3±0.9	0.007
ZrO ₂	Zr–O	8.3±0.2	2.28±0.02	12.6±3.2	0.6±3.0	0.019
	Zr–Zr	6.2±0.2	3.46±0.01	6.9±1.5	-6.4±2.6	
Zr/NC	Zr–N	4.1±0.1	2.22±0.01	7.8±2.2	-0.3±1.8	0.014

Note: S_0^2 is the amplitude reduction factor; CN is the coordination number; R is the interatomic distance or bond length between central atoms and surrounding coordination atoms; σ^2 is the Debye-Waller factor to account for thermal and structural disorders; ΔE is the inner potential correction; R factor is the goodness of fitting.

Table S3 Comparison of various catalysts for the TH of HMF to BHMF.

Catalyst	Alcohol	Temperature	Time (h)	Conversion (%)	Yield (%)	TOF (h ⁻¹)	Reference
Zr-TN	<i>i</i> PrOH	100	5	95	89	0.73	1
Zr-AZN	<i>i</i> PrOH	100	4	96	90	0.89	2
Zr-DTPA	<i>i</i> PrOH	140	4	99	95	1.35	3
Zr-FDCA	<i>i</i> PrOH	140	8	97	87	1.62	4
Zr-CTS	<i>i</i> PrOH	120	4	99	97	1.67	5
Zr-LS	<i>i</i> PrOH	100	2	98	89	2.02	6
Zr-XDPA	<i>i</i> PrOH	120	2	99	93	2.34	7
Zr-DTMPA	<i>i</i> PrOH	140	2	91	82	2.61	8
Zr-ATMPA	<i>i</i> PrOH	140	2	99	98	3.55	9
Zr-BTC	<i>i</i> PrOH	82	2	98	96	4.60	10
Zr-HTC	<i>i</i> PrOH	120	4	100	99	5.61	11
Zr-EL	<i>i</i> PrOH	140	4	100	99	10.86	12
Zr/NC	<i>i</i> PrOH	130	5/2	100	100	124.26	This work

Note: TOF = (mole of BHMF)/(mol of metal × time).

Table S4 TH of HMF to BHMF over Z/NC in various deuterated *i*PrOH.

Entry	Alcohol	Molecular formula	KIE
1	<i>i</i> PrOH	CH ₃ CH(OH)CH ₃	—
2	<i>i</i> PrOH-OD	CH ₃ CH(OD)CH ₃	1.087
3	<i>i</i> PrOH-D ₈	CD ₃ CD(OD)CD ₃	2.152

Reaction conditions: 0.25 g HMF, 19.75 g alcohol, 0.1 g Zr/NC, 130 °C, 150 min.

References

- 1 Y. Leng, L. Shi, S. Du, J. Jiang and P. Jiang, *Green Chem.*, 2020, **22**, 180-186.
- 2 Q. Peng, X. Li, X. Wang, Y. Li, Y. Xia, X. Liu and H. Wang, *Sustain. Energ. Fuels*, 2021, **5**, 4069-4079.
- 3 L. Hu, S. Liu, J. Song, Y. Jiang, A. He and J. Xu, *Waste Biomass Valori.*, 2020, **11**, 3485-3499.
- 4 H. Li, X. Liu, T. Yang, W. Zhao, S. Saravanamurugan and S. Yang, *ChemSusChem*, 2017, **18**, 1761-1770.
- 5 T. Wang, H. Xu, J. He and Y. Zhang, *New J. Chem.*, 2020, **44**, 14686-14694.
- 6 S. Zhou, F. Dai, Z. Xiang, T. Song, D. Liu, F. Lu and H. Qi, *Appl. Catal. B: Environ.*, 2019, **248**, 31-43.
- 7 H. Li, Z. Fang, J. He and S. Yang, *ChemSusChem*, 2017, **10**, 681-686.
- 8 L. Hu, N. Li, X. Dai, Y. Guo, Y. Jiang, A. He and J. Xu, *J. Energy Chem.*, 2019, **37**, 82-92.
- 9 H. Li, J. He, A. Riisager, S. Saravanamurugan, B. Song and S. Yang, *ACS Catal.*, 2016, **6**, 7722-7727.
- 10 A. H. Valekar, M. Lee, J. W. Yoon, J. Kwak, D. Y. Hong, K. R. Oh, G. Y. Cha, Y. U. Kwon, J. Jung, J. S. Chang and Y. K. Hwang, *ACS Catal.*, 2020, **10**, 3720-3732.
- 11 A. He, L. Hu, Y. Zhang, Y. Jiang, X. Wang, J. Xu and Z. Wu, *ACS Sustain. Chem. Eng.*, 2021, **9**, 15557-15570.
- 12 Y. Zhang, X. Shen, L. Hu, Z. Wu, X. Wang and Y. Jiang, *Biomass Convers. Bior.*, 2022, DOI: 10.1007/s13399-022-02381-9.